

CAAP Quarterly Report

[03/31/2025]

Project Name: "All-in-One Multifunctional Cured-In-Place Structural Liner for Rehabilitating of Aging Cast Iron Pipelines"

Contract Number: 693JK32250009CAAP

Prime University: North Dakota State University

Prepared By: [Ying Huang, ying.huang@ndsu.edu, 701-231-7651]

Reporting Period: [12/27/2024– 03/27/2025]

Project Activities for Reporting Period:

In the 9th quarterly report, Tasks 2.1, 2.2, 3.1, 3.2, 3.3, 3.4, 4.1, 4.2, and 5.1 were carried out as proposed. During the current reporting period (Q10), the research team has continued making steady progress on the selected tasks. Key activities accomplished during this quarter are summarized in this report.

Task 2.1 Preparation of Vitrimer Epoxy Resins, Characterization, and Optimization of the Processing and Curing Conditions (95%): In the last quarter, catalysts were incorporated into the self-healing polymers to optimize the formulation. The research team (Dr. Long Jiang and Austin Knight, Ph.D. student at NDSU) further investigated methods to enhance catalyst dissolution and adjusted the formulations to optimize the thermal properties of the self-healing polymers. The key findings are summarized below:

- (1) Preliminary Investigation into Dissolving the Transesterification Catalyst: The complete dissolution of the transesterification catalyst in a solvent would prevent the UV-inhibitory effects of the catalyst. The solubility of the catalyst was investigated in water, acrylic acid, acetic acid, glycerol, ethylene glycol, and the methacrylate diluent. Of these, water performed the best followed by ethylene glycol and glycerol. None of these solvents, however, are reactive and would act as plasticizers and weaken the polymer. A literature revealed a reactive diluent that has been used to dissolve the catalyst for UV-cured formulations that may be investigated in the future if the UV-inhibition continues to be a prominent problem.
- (2) Investigation into the Reactive Diluents Thermal Properties: To evaluate how the reactive diluent affects the thermal properties of the polymer, dilatometry tests were conducted on the diluents as homopolymers. The methacrylate diluent exhibited a significant exponential strain increase starting around 120°C, a behavior not observed with the acrylate diluent, likely due to impurities. These impurities were subsequently reduced by performing hexane extractions (Figure 1(a)). After extraction cycles, the acrylate monomer showed increased purity but exhibited a lower relaxation temperature (~50°C) when mixed with the purified methacrylate diluent (Figure 1(b)). This purified mixture will serve as the reactive diluent in subsequent tests, pending receipt of a new, potentially purer batch of acrylate diluent.

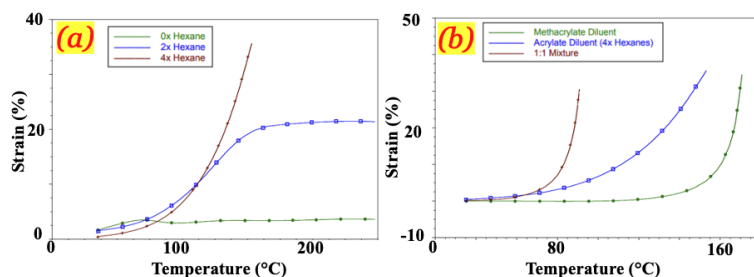


Figure 1. The dilatometry results for (a) RDA after various degrees of purification and (b) RDMA as received, RDA after purification, and a 1:1 mixture of the two diluents.

(3) Increasing Catalyst Content in Methacrylate Diluent: To see if the acrylate diluent was the cause for the decreased vitrimer properties due to impurities, the same formulations with increasing catalyst content were tested with the methacrylate diluent. A small decrease in the onset temperature was seen with increasing catalyst content but the vitrimer properties are still not very pronounced (Figure 2).

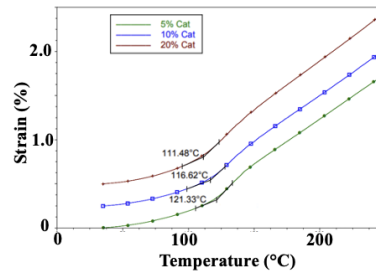


Figure 2. The dilatometry results for the DFA RDMA formulations with varied catalyst concentrations.

(4) Lowering Acrylate Crosslinker Content: Lowering the crosslinker (DFA) content reduces the number of crosslinked bonds requiring dynamic exchange, potentially enhancing material relaxation. The crosslinker content was adjusted by increasing the RDMA-to-DFA ratio, thus systematically increasing diluent (RDMA) content. Formulations containing 10 mol% catalyst showed a minor increase in strain when RDMA content rose from 2 to 16 mol% (Figure 3(a)). Significantly greater strain was observed when the RDMA content increased from 2 to 100 mol%, demonstrating similar strain at room temperature but an increase from approximately 2.5% to 15% strain above the vitrimer transition temperature ($\sim 195^\circ\text{C}$) (Figure 3(b)).

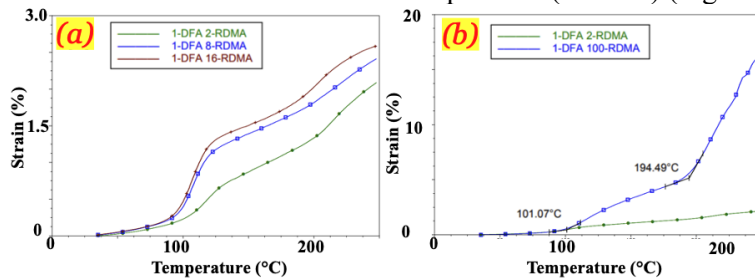


Figure 3. The dilatometry results for (a) 10 mol% catalyst 1:2, 1:8, and 1:16 crosslinker to diluent ratio and (b) 20 mol% catalyst 1:2 and 1:100 crosslinker to diluent ratio.

Task 3.1 High Mechanical Performance (95%) and Task 3.2 Enhanced bonding performance (80%): During this reporting period, the research team (Dr. Ying Huang, Dr. Xingyu Wang, and Muhammad Imran Khan, Master student from NDSU) investigated on other 0-D nanoparticles to expand the selection available for this project. The key findings are summarized below:

(1) Mechanical Properties of Composite with Selected 0-D Nanoparticles (NPs): Based on previous results, the ND formulation demonstrated significant improvements compared to CNT and GNP formulations, likely due to the dimensional characteristics of ND. While continuing the optimization of self-healing polymers in Task 2, the research team is further exploring additional 0-D nanoparticles to expand the selection available for this project. Presented below (Figure 4) are the current obtained tensile properties of the formulations incorporating ZnO, CuO, and TiO₂ nanoparticles with concentrations ranging from 0.5 to 1.5 wt.%.

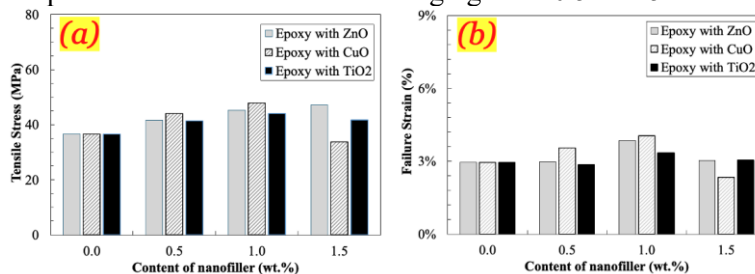


Figure 4. Results of the tensile properties test for epoxy with ZnO, CuO, and TiO₂ nanoparticles.

Task 3.3 Reducing the Permeability and Investigating the Interfacial Bonding Chemical Analysis (80%): Previously, the research team (Dr. Liangliang Huang, Hao Yuan, Ph. D. student from University of Oklahoma) employed the REACTOR method to perform reactive molecular dynamics simulations for

modeling the transesterification reaction in vitrimer systems. During the current reporting period, we implemented the OPLS-AA force field and conducted targeted optimizations specific to our model. In addition to simulating the transesterification reaction between bisphenol A-glycidyl methacrylate (Bis-GMA) and 2-Hydroxyethyl Methacrylate (2-HEMA), we also successfully modeled the polymerization process of these monomers through molecular dynamics simulations.

- (1) Force Field Optimization: In subsequent simulations, we adopted the OPLS-AA force field due to its superior predictive accuracy and integrated it with the Type Label framework method; therefore, streamlining workflows and improving compatibility with simulation tools such as REACTER. It is worth noting that the classical force field does not consider the electronic polarization or charge transfer effect in its parameters, making it challenging to acquire accuracy in transport properties comparable to experimental results. At present, the alternative approach to overcome such an issue is to scale the atomic charge to reduce the magnitude of the electrostatic interactions. Accordingly, here we used a scaling factor of 0.8 to include the effect of polarization during the molecular dynamics simulation. In addition, the positively charged hydrogen atom on the Bis-GMA molecule was simultaneously attracted to both adjacent oxygen atoms, resulting in molecular instability. To address this issue, the charge of the hydrogen atom was set to zero, and the negative charge of the bonded oxygen atom was reduced, enabling local stabilization of the molecule. Similar adjustments were made to the hydroxyl group on the 2-HEMA molecule to ensure stability during simulations, the final charge distribution on the molecule is shown in Figure 5.

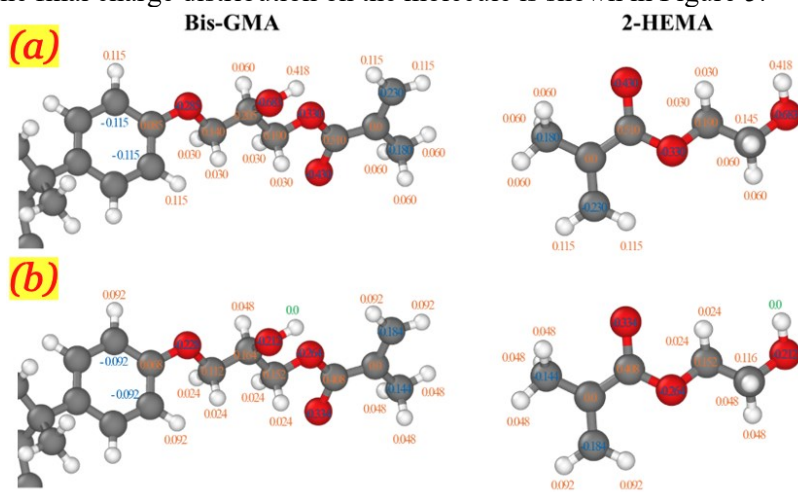


Figure 5. (a) Charge parameters from OPLS-AA force field, and (b) Modified charge parameters

- (2) Polymerization: After defining the map file and template files required for the reaction simulation, we constructed a system consisting of 10 pairs of Bis-GMA and 2-HEMA molecules, as presented in Figure 6. The reaction was successfully simulated under conditions of 300 K, 1 atm pressure, and a test density of 0.1 g/cm³. To further explore the effect of temperature on the reaction dynamics, we conducted additional tests by varying the temperature while keeping other parameters constant. Simulations were carried out at 300 K, 600 K, and 900 K. The results revealed that at elevated temperatures of 600 K and 900 K, the simulation system encountered errors related to missing bonds or atoms. We believe that these errors are due to the increased kinetic energy at higher temperatures, which causes atoms to move more rapidly and, in some cases, drift too far apart during the reaction process. This excessive separation between atoms likely disrupts the bond formation necessary for the reaction, leading to inaccuracies in the simulation.

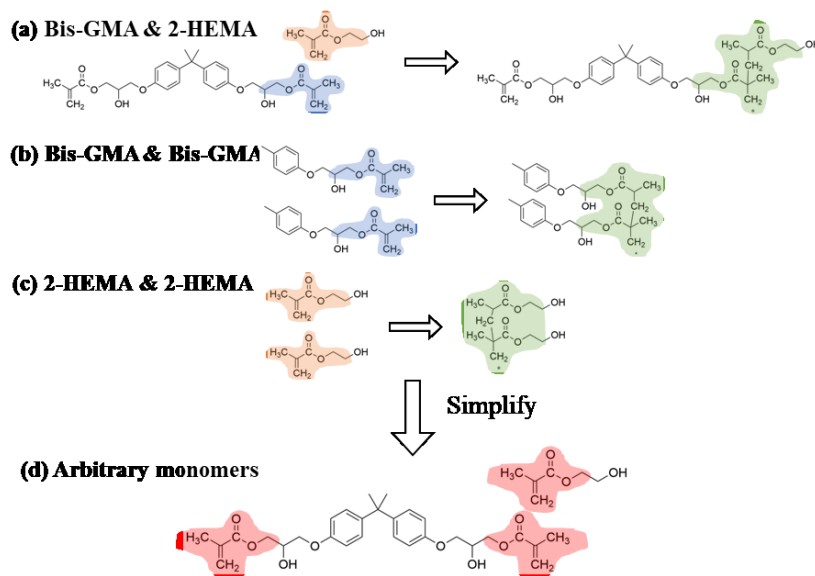


Figure 6. Examples of reactive schemes.

Note: The orange and blue regions represent reactant topologies of 2-HEMA and Bis-GMA, respectively. In order to reduce the number of reaction templates required, we simplified their reactant topologies to the same region (red region).

Task 3.4 Finite Element Numerical Analysis to Guide the Design of the Developed High-performance Healable CIPP Structural Liner (90%): During this reporting period, the research team (Dr. Chengcheng Tao and Junyi Duan, Ph.D. student from Purdue University) further advanced the finite element analysis (FEA) of pipelines rehabilitated with CIPP liners to investigate the pipe-liner system's response under impact loading. The FEA results were validated using experimental data obtained in Task 4.1. Key findings are summarized below:

- (1) Finite Element Analysis of External Impact on Liner-Rehabilitated Substrate: Finite element analysis (FEA) is conducted to investigate external impacts on the liner-rehabilitated substrate, which are classified into static and dynamic categories. A solid C440 stainless steel ball with a radius of 50.8 mm is used as the impactor for the static impact simulation. The three-layer plate structure is modeled using 8-node linear solid-shell elements with enhanced surface stress visualization (C3D8S) in ABAQUS. The C3D8S element is particularly suitable for thin plates and has proven effective in capturing buckling behavior across plates with varying thicknesses and aspect ratios. The interfacial conditions between layers are modeled as perfectly bonded (tied), assuming a fully cured adhesive layer that ensures strong adhesion between adjacent materials. Four points (Points #1 to #4) were experimentally tested. Strain contours under static impact applied at the center (Point #1) are used for demonstration, showing results from both experimental measurements (Figure 7 (b)) and FEA simulations (Figure 7 (c)). The comparison indicates strong agreement between experimental and simulated strain distributions for the central impact case. For the other three points, while minor discrepancies are noted, the strain data comparison in Table 1 confirms the overall accuracy and reliability of the FEA model.

| Location | Source | Max. Strain ($\mu\epsilon$) |
|----------|------------|-------------------------------|
| Point 1 | Experiment | 159 |
| | FEA | 164 |
| Point 2 | Experiment | 183 |
| | FEA | 196 |
| Point 3 | Experiment | 98 |
| | FEA | 104 |
| Point 4 | Experiment | 115 |
| | FEA | 115 |

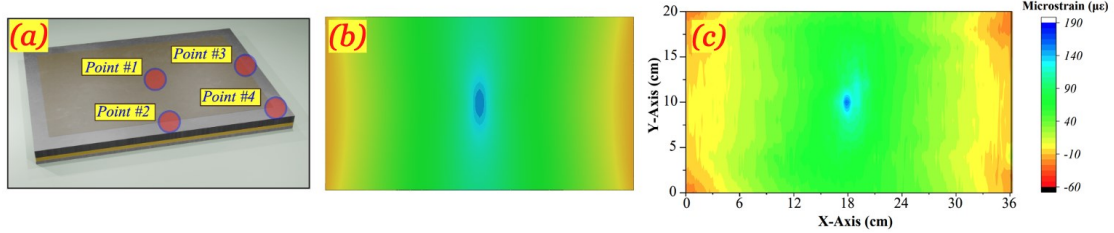


Figure 7. Strain comparison results at Point #1 (a) illustration of the impact locations, (b) simulation result, and (c) experimental result.

Task 4.1 Development of Embedded Distributed Fiber Optic Sensors for Self-sensing Structural Liner (90%), and **Task 4.2** Investigating the Load Transfer between Layers of the CIPP Liner and the Cast-iron Substrate (75%): During this reporting period, the research team (Dr. Ying Huang and Dr. Xingyu Wang) continued experimental investigations on the smart-liner system under impact loading. The objectives were to accurately identify the impact location, analyze the strain field, and develop a digital twin model representing deformation in the smart-liner system. The key findings are summarized below:

- (1) Developed Method for Digital Twin Model under Impact Actions: The creation of the digital twin model follows a new procedure outlined in Figure 8, illustrating the deformation visualization process for the smart-liner system. Initially, static or dynamic loads are applied to the smart-liner protected steel plate, and distributed fiber optic sensors embedded in the liner capture real-time strain data. The collected strain data are then converted from one-dimensional fiber coordinates into parametric coordinates mapped onto the physical structure, allowing spatial representation of the strain distribution. Subsequently, a machine learning algorithm compares the strain patterns with finite element model predictions to identify deformation behaviors under applied loads. The final deformation visualization provides an intuitive representation of structural response, integrating real-time sensing, finite element analysis, machine learning, and digital twin technology. This approach demonstrates the smart-liner system’s effectiveness as an advanced structural monitoring and analytical tool.

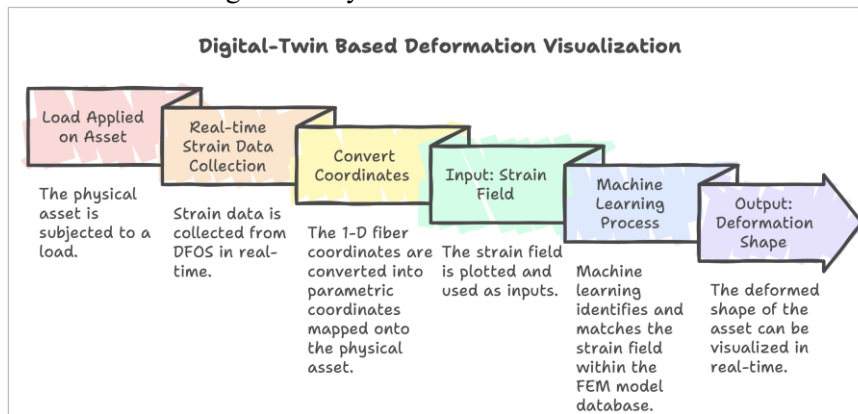


Figure 8. The process of creating a digital twin model for deformation visualization.

- (2) Digital twin-based Deformation Visualization: The obtained strain fields were analyzed using a machine learning algorithm to correlate experimental data with FEA predictions, enabling digital twin deformation visualization. As illustrated in Figure 9, experimental strain fields effectively matched corresponding simulated fields across all four loading points, confirming the algorithm’s reliability and robustness. This matching facilitated accurate reconstruction of the specimen’s deformation, directly linking strain fields to deformation distribution and enabling successful digital twin visualization. The integration of experimental data with digital modeling demonstrates this method’s potential for real-time structural monitoring. The entire process—including strain

data collection, strain field generation, and deformation visualization—was completed within seconds of computational time. If integrated with real-time data transmission from the DFOS interrogator, the approach could achieve near-instantaneous deformation visualization, significantly enhancing its capability for structural health monitoring and safety assessment.

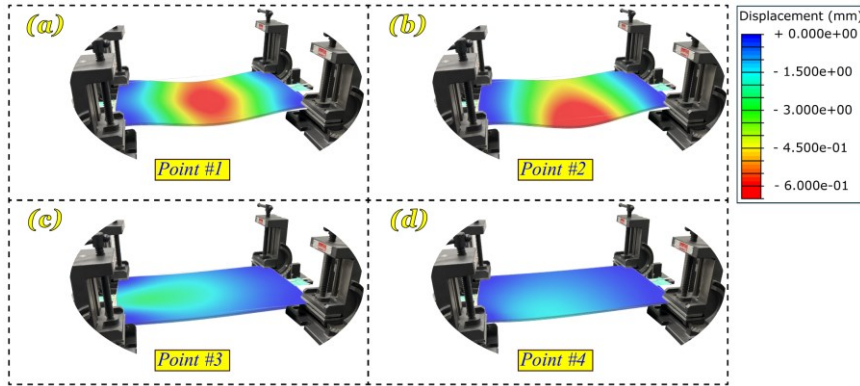


Figure 9. Digital twin model illustrating the deformation of the liner-protected plate specimen under loading at Point #1 to Point #4.

Task 5.1 Development of CIPP Liner Risk Index for the Pipeline Integrity Management Enhanced by AI Algorithms (70%): During this period, the research team (Dr. Chengcheng Tao and Huaixiao Yan, Ph.D. student from Purdue University) conducted a risk assessment using datasets generated from fiber optic sensors (Task 4). A method for optimizing sensor deployment based on sensitivity analysis was developed, with key findings summarized below:

- (1) Sensitivity Analysis to Guild the DFOS Installation: Distributed Fiber Optic Sensors (DFOS) offer extensive sensing capabilities; however, their deployment poses significant challenges due to varying structural geometries and specific monitoring objectives, often requiring complex installation procedures and specialized data-processing techniques. Additionally, DFOS generate massive datasets, especially at high spatial resolutions; for instance, a 5-meter DFOS with 1.3 mm resolution at 10 Hz produces over 138 million data points per hour. Therefore, conducting sensitivity analyses to optimize sensor placement is essential for measurement efficiency. In this study, we conducted a sensitivity analysis to optimize DFOS deployment on a CIPP liner subjected to buckling loads. A weighted K-means clustering algorithm was applied, assigning weights to measurement points based on their strain gradients to emphasize regions of high sensitivity. Through iterative clustering adjustments, optimal sensor locations were identified. Starting from 4344 measurement points at a 0.65 mm spatial resolution, the number of points was gradually reduced. Figure 10 illustrates the optimized sensor locations under four different scenarios.

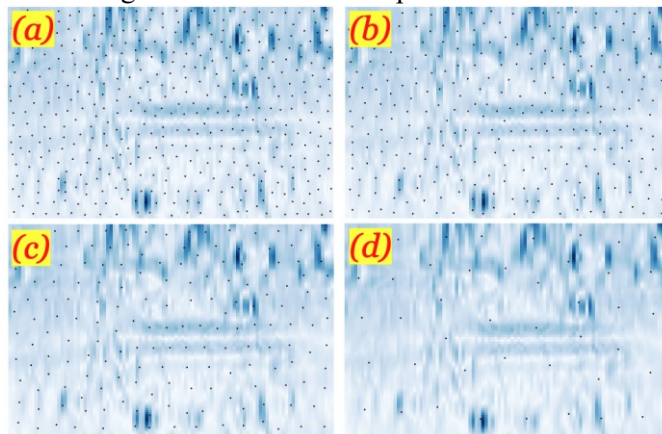


Figure 10. Optimal measurement points locations with a reduced number of measurement points: (a) 10%, (b) 7%, (c) 4%, and (d) 1% of the maximum points.

Note: The background represents the strain gradient, while the black dots indicate optimal sensor locations. This method guides DFOS installation and optimization by effectively covering regions with sufficient black points.

Project Financial Activities Incurred during the Reporting Period:

The cost breakdown during the reporting period according to the budget proposal is shown in Table 2.

Table 2. Cost breakdown

| Category | Amount spent during Q10 |
|---------------------------|-------------------------|
| Personnel | |
| Faculty | \$0.00 |
| Postdoc | \$1,499.90 |
| Students (RA and UR) | \$10,900.00 |
| Benefits | \$805.55 |
| Operating Expenses | |
| Travel | \$0.00 |
| Materials and Supplies | \$1,258.52 |
| Recharge Center Fee | \$3,038.01 |
| Consultant Fee | \$1,275.00 |
| Subcontracts | \$33,843.02 |
| Indirect Costs | \$8,449.66 |

Project Activities with Cost Share Partners:

The Match fund from NDSU for this project is coming from the tuition of the associated graduate students during their work on this project. During the reporting period (Q10), Zahoor Hussain (100%), Muhammad Imran Khan (100%), Austin Knight (100%), and Tofatun Jannet (100%) were working on the project. The tuition for the four students during Q10 was estimated to be \$12,520 at a rate of \$463.73 per credit.

Project Activities with External Partners:

During this reporting period, George Ragula, our industry consultant, attended all the bi-weekly meetings with the research team.

Potential Project Risks:

No potential risks were noticed during this reporting period.

Future Project Work:

The research team will continue working on Tasks 2.1, 2.2, 3.1, 3.2, 3.3, 3.4, 4.1, 4.2 and 5.1.

Potential Impacts on Pipeline Safety:

As proposed in Q9, the research team has further advanced the development of self-healing polymers by incorporating catalysts and adjusting formulations to enhance thermal properties; thereby improving self-healing performance at lower temperatures. Additionally, significant progress was achieved in molecular dynamics simulations by adopting and optimizing a new force field, successfully modeling both the transesterification reaction and the polymerization process of self-healing polymers. Additionally, Finite Element Analysis (FEA) modeling was integrated closely with experimental studies, focused on evaluating the behavior of the smart-liner system under impact loading. An AI-driven approach was also developed to identify impact locations and generate accurate digital twin models for deformation visualization. Furthermore, sensitivity analysis was performed to optimize DFOS sensor deployment, ensuring cost-effective monitoring. These findings offer critical insights to enhance performance, reliability, and failure prevention during the design and manufacturing stages of CIPP liner systems.